

## ANALYSIS OF SEISMIC ATTRIBUTES TO ENHANCE A BOTTOM SIMULATING REFLECTOR (BSR) IN THE GAS HYDRATE AREA OF UMITAKA SPUR, EASTERN MARGIN OF JAPAN SEA

Eloíse Helena Policarpo Neves <sup>1\*</sup>, Cleverson Guizan Silva <sup>1</sup>,  
Ryo Matsumoto <sup>2</sup>, and Antonio Fernando Menezes Freire <sup>1</sup>

<sup>1</sup>Universidade Federal Fluminense – UFF, Department of Geology and Geophysics; Exploratory Interpretation and Reservoir Characterization Group (GIECAR), Av Gen. Milton Tavares de Souza, s/n, Boa Viagem – Niterói, RJ, Brazil – E-mails: [eloisehpn@id.uff.br](mailto:eloisehpn@id.uff.br), [cguizan@id.uff.br](mailto:cguizan@id.uff.br), [fernando\\_freire@id.uff.br](mailto:fernando_freire@id.uff.br)

<sup>2</sup>Meiji University, Tokyo, Japan – E-mail: [ryo\\_mat@meiji.ac.jp](mailto:ryo_mat@meiji.ac.jp)

**ABSTRACT.** This work aims to evaluate the best seismic attributes to use to identify the Bottom Simulating Reflector (BSR) of Umitaka Spur, a well-known gas hydrate area in Joetsu Basin, Japan. For this purpose, it uses 2D single-channel seismic data from cruises NT07-20 and NT08-09 provided by the Japan Agency for Marine-Earth Science and Technology (JAMSTEC). The methodology used for the qualitative analysis of six seismic attributes to highlight the BSR was done using Schlumberger's Petrel software. These attributes were Envelope, RMS Amplitude, Amplitude Volume Technique (tecVA), Relative Acoustic Impedance, Spectral Decomposition and Instantaneous Frequency. Thus, this study was fundamental to investigate gas hydrates occurrence through the seismic assessment of some geophysical property (amplitude and frequency) and the geological attributes that highlighted the faults of the complex local geology. The application of these attributes can be used in other areas providing an effective tool to enhance the recognition of BSR all over the world.

**Keywords:** gas hydrate stability zone; instantaneous frequency; instantaneous frequency; spectral decomposition; relative acoustic impedance; tecVA

## INTRODUCTION

Investigating the presence of gas hydrate in the subsurface is important to mitigate geological hazards and to exploit this unconventional energy resource that is cleaner than oil and coal (Kvenvolden, 1993; Chong et al., 2016). The seismic reflection method is the most widely used geophysical method of exploration. For instance, in marine seismic profiles, the Bottom Simulating Reflector (BSR) is known to indirectly demarcate the Base of Gas Hydrate Stability Zone (BGHSZ). BSR is a seismic reflector that is parallel, with a reverse polarity in relation to the seafloor reflector, which often crosscut the bedding plane of the host sediments (Buffett, 2000). However, identifying the true BSR can be difficult without the application of seismic attributes, because sometimes it appears weak and patchy.

Seismic attributes are the main tools used to predict lithology of seismic reflection data, which can act as filters that quantify properties of seismic images (Taner, 2001). There are several studies that apply seismic attributes in order to investigate the presence of gas hydrate in different regions of the world (e.g., Hato et al., 2006; Santos et al., 2009; Oliveira and Oliveira, 2009; Joshi et al., 2017; Aguiar et al., 2019, 2021). Thus, this work aims to evaluate the best seismic attributes for identification of BSR in a widely studied gas hydrate site, Umitaka Spur, Joetsu Basin, Japan (Fig. 1). For this purpose, we used 2D seismic lines provided and already migrated by the Japan Agency for Marine-Earth Science and Technology (JAMSTEC). These data are from cruises NT07-20 and NT08-09, carried out in 2007 and 2008 respectively.

Since 2004, studies focusing on the origin and significance of shallow, massive to fracture-filling gas hydrates have begun in Joetsu Basin by a research consortium of universities, national institutes and industries (Matsumoto et al., 2011). Thus, miscellaneous studies involving gas hydrates issues in this area have been carried out, such as geophysical (e.g., Saeki et al., 2009; Santos et al., 2009), geological and geochemical analysis (e.g., Matsumoto et al. 2009, 2011, 2017; Freire et al., 2011; Snyder et al., 2020). The contribution of this study is the knowledge coming from the analysis of six seismic attributes to enhance BSR in seismic sections from this area, which is also useful for others areas of the world.

### **GEOLOGIC SETTING**

The Joetsu Basin is located on the eastern margin of Japan Sea, southwest of Sado Island (Fig.1). The Japan Sea is a composite back-arc basin formed behind the Japanese island-arc system initiated by the rifting of the eastern margin of the Eurasian Continent (Suzuki, 1979 in Okui et al., 2008), accompanied respectively by clockwise and counter-clockwise of southwestern and northeastern Japan, during the early Miocene (Otofuji et al., 1985 in Nakajima et al., 2014). The Joetsu Basin was also formed in the Miocene. During the middle Miocene, due to initial rifting, there was a marine transgression, thus, the Joetsu Basin was filled chiefly by deep-marine siliceous shale with minor sandstone (Okui et al., 2008). During this epoch, a high production of organic matter under anoxic conditions favored the development of good source rocks from the Nanatani (16-12.5 Ma) and Lower Teradomari (12.5-8 Ma) formations (Hirai et al., 1995, in Okui et al., 2008).

From around 10 Ma to 7 Ma, the Japan Sea was tectonically stable (Freire et al., 2011). Thus, coarse-grained sediments (tuffaceous sandstone and siltstone) were transported to the Joetsu Basin and deposited as turbidites fans, which became primary reservoirs in the Lower Teradomari (12.5-8 Ma), the Upper Teradomari (8-5.5 Ma) and the Shiiya (5.5-3.5 Ma) formations (Sato et al., 1987 in Okui et al., 2008). Overlapping the Shiiya Formation, the Nishiyama (3.5-1.3 Ma) Formation is composed mainly of fine mudstones with sandstones, including also volcanic rocks, such as dacites and andasites (Freire et

al., 2011). The most recent formation is Haizume, it has been deposited since the late Pliocene and it is dominated chiefly by clayey sediments (Son et al., 2001 in Freire et al., 2011).

The Umitaka Spur is an anticline with a nearly N-S trend formed since the middle Pliocene, when the tectonic style changed from extensional to compressive (Takeuchi, 1996 in Freire et al., 2011). The spur encompasses an area of 43 km<sup>2</sup> (Freire et al., 2011). The occurrence of seeps and plumes escaping from the seafloor indicates the lack of trapped gas (Matsumoto, 2005; Aoyama and Matsumoto, 2009 in Freire et al., 2011). Although the weak efficiency of both seal and trap for conventional oil and gas production, this scenario is perfect for gas hydrates reservoirs due to the gas supply (Freire, 2010).

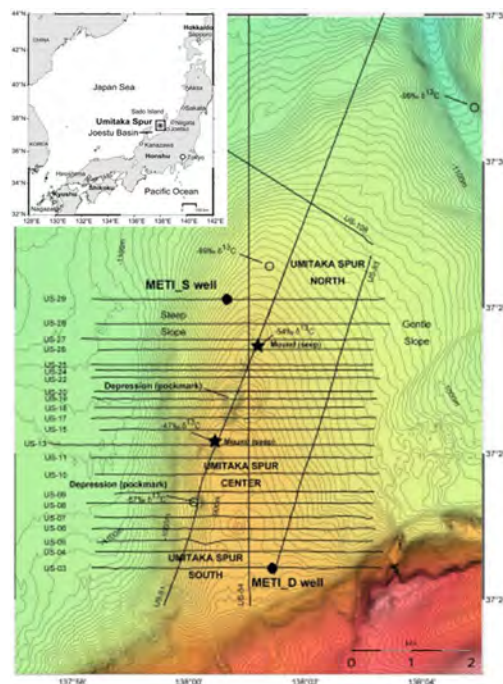


**Figure 1** – Location map of the seismic survey. Map of the seafloor relief of the Umitaka Spur showing mounds and depressions in an NE-SW trend. Stars indicate seep locations. Open circles indicate carbon isotope analyses of sediments (Freire, 2010). Hot colors correspond to shallow zones while cold colors correspond to deep zones. The contour lines in the green colors are around 1100m while in the yellow colors they are around 900m below sea level.

## METHODS

Initially, all of the 2D seismic lines provided by the JAMSTEC were loaded. Then, a quality control of these seismic sections was carried out, such as the evaluation of possible noises in the acquisition.

After that, the main step consisted of the application of six seismic attributes. First, we applied two seismic attributes that measure amplitude (Envelope and Root-Mean-Square Amplitude). Then, we applied Amplitude Volume Technique (tecVA), which consisted of applying a phase shift of -90° in RMS Amplitude attribute (Bulhões and Amorim, 2005).

Then, Relative Acoustic Impedance was used to highlight seismic reflectors. Before applying the frequency attributes, an analysis of the frequency spectrum was generated to obtain on the frequency domain in each seismic section. Spectral Decomposition and Instantaneous Frequency were applied. Finally, the BSR of each 2D seismic section was interpreted by analyzing the results of these six seismic attributes.

## RESULTS AND DISCUSSION

After importing the data, a quality control was carried out and only one seismic section was discarded, which was SP.2(4\_FSP) from the NT07-20 cruise. Therefore, twenty-eight 2D seismic sections were used in this work in total. Then, a seafloor grid was generated through the interpretation of the seafloor horizon of these 2D seismic sections.

After that, the application of seismic attributes to enhance BSR on all seismic sections began. However, due to the large number of seismic sections, only the results of the SP.2(19\_FSP) and SP.2(51-1\_FSP) will be addressed here. They were chosen for this assessment because seismic section SP.2(19\_FSP) shows a very visible pockmark and SP.2(51-1\_FSP) is a strike line.

Note that (Fig. 2) SP.2(19\_FSP) has blanking zones. From previous work, such as Freire et al., 2011, we know that the BSR is located approximately between 1.5 and 1.8 s TWT in the SP.2(19\_FSP) seismic section. However, if we did not have any prior information from the study area, note that it would be difficult to interpret where the true BSR would be, because it has more than one reflector close and parallel to the seafloor with a strongly negative impedance contrast. So, applying seismic attributes is important to reduce these interpretation concerns.

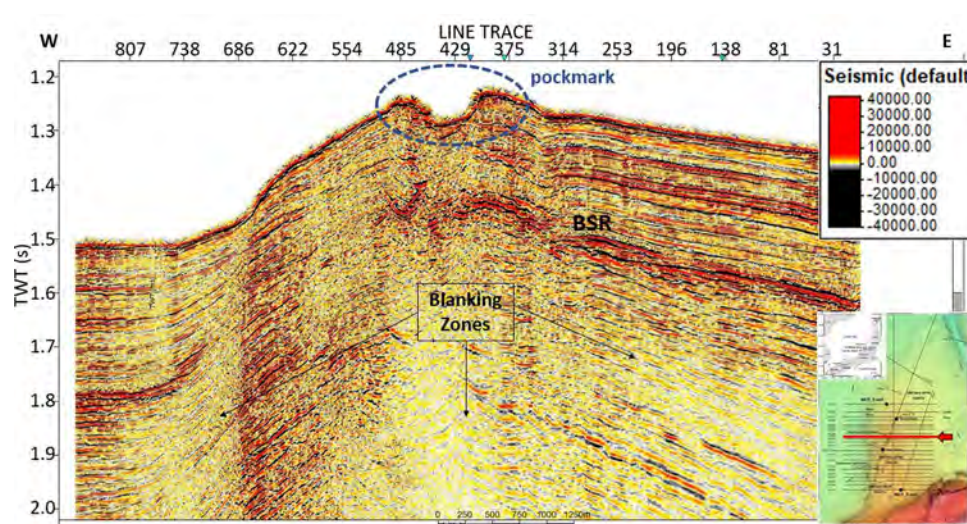


**Figure 2** – 2D Single-Channel Seismic (SCS) section SP.2(19\_FSP) from NT07-20 cruise. The diffractions in the central part have not been fully collapsed in the seismic processing. Note a deep pockmark in the central portion, directly related to the occurrence of gas hydrates at the seafloor.

## Envelope

When applying the Envelope attribute all values become positive. It measures total instantaneous energy (Taner et al., 1979). Note in Figure 3 that all high acoustic impedance contrast were highlighted, such as seismic reflectors H-I and H-II of the Haizume Formation, BSR and the flat spot below it, probably indicates a free gas/water contact (Freire et al., 2011), but as the data are presented in vertical time scale, it demands a caution in this interpretation.

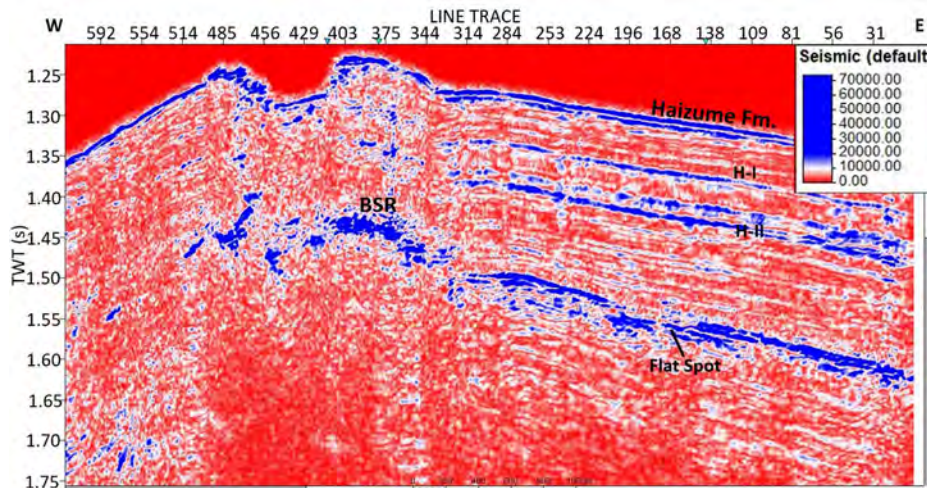


**Figure 3** - SP.2(19\_FSP) with Envelope attribute. Blue color highlights the highest amplitudes while red color corresponds to values close to zero.

## RMS Amplitude and Amplitude Volume Technique

The Amplitude Volume Technique (tecVA) consisted of applying a phase shift of  $-90^\circ$  in RMS Amplitude. Thus, before obtaining the result of the application of the tecVA, we have the result of the RMS Amplitude. The RMS Amplitude highlighted extreme amplitude anomalies and it has an effect similar to the application of the envelope (Fig. 4).

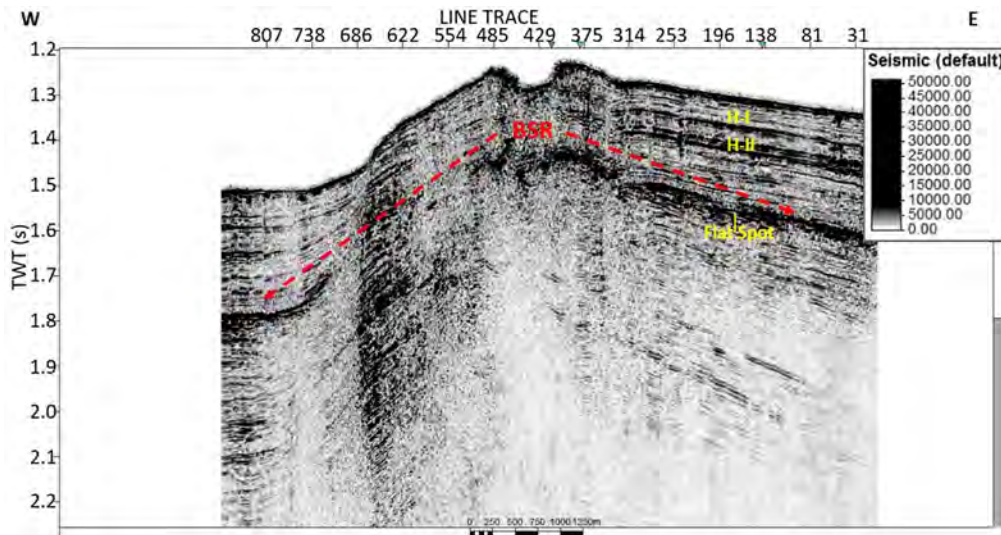


Figure 4 – SP.2(19\_FSP) with RMS Amplitude.

Then phase shift of  $-90^\circ$  was applied (Fig. 5). This attribute created a pseudo-relief effect, thus highlighting the BSR, which is laterally discontinuous.

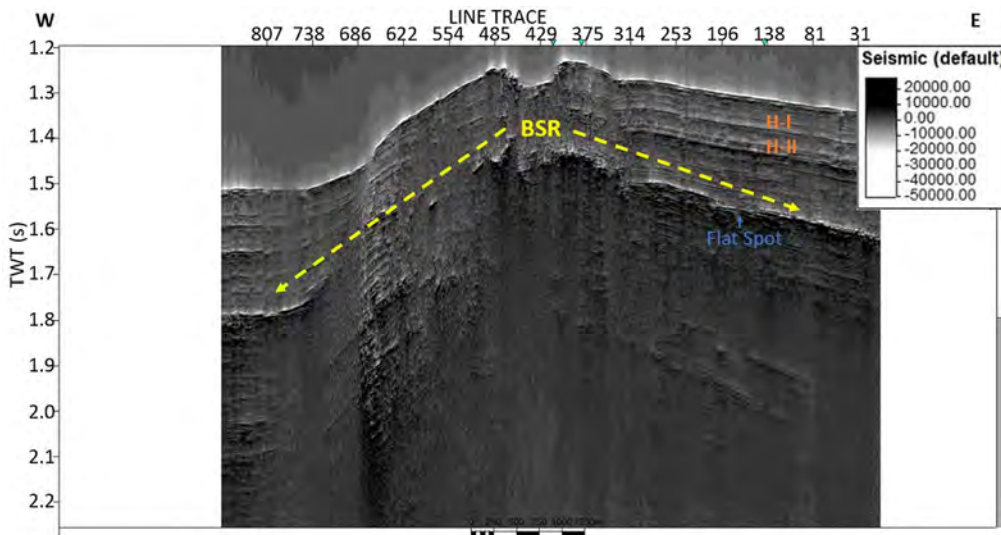
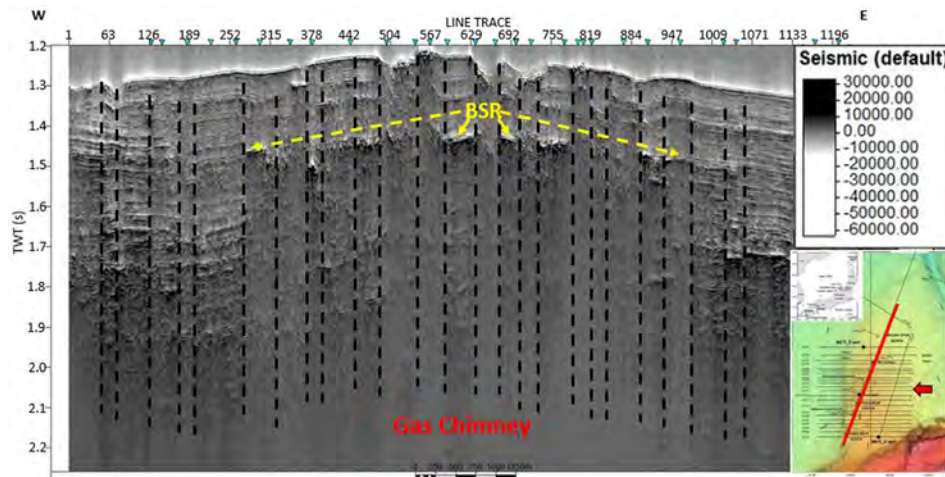


Figure 5 - SP.2(19\_FSP) with Amplitude Volume Technique.

In addition, it was useful to enhance the high impedance contrasts and discontinuities. For instance, tecVA was good to highlight the strike line fault system SP.2(51-1\_FSP) (Fig. 6).



**Figure 6** - SP.2(51-1\_FSP) with Amplitude Volume Technique. The dashed lines mark the interpretation of vertical faults. The blanking zones are associated with gas chimneys.

### Relative Acoustic Impedance

Comparing the result obtained (Figure 7) with Figure 2, it can be noted that RAI attribute highlighted all the seismic reflectors. Despite highlighting non-collapsed diffractions, there was an enhancement of the weak reflectors of the blanking zones, where there is presence of free gas. In addition, note that BSR appears stronger than H-I and H-II reflectors.

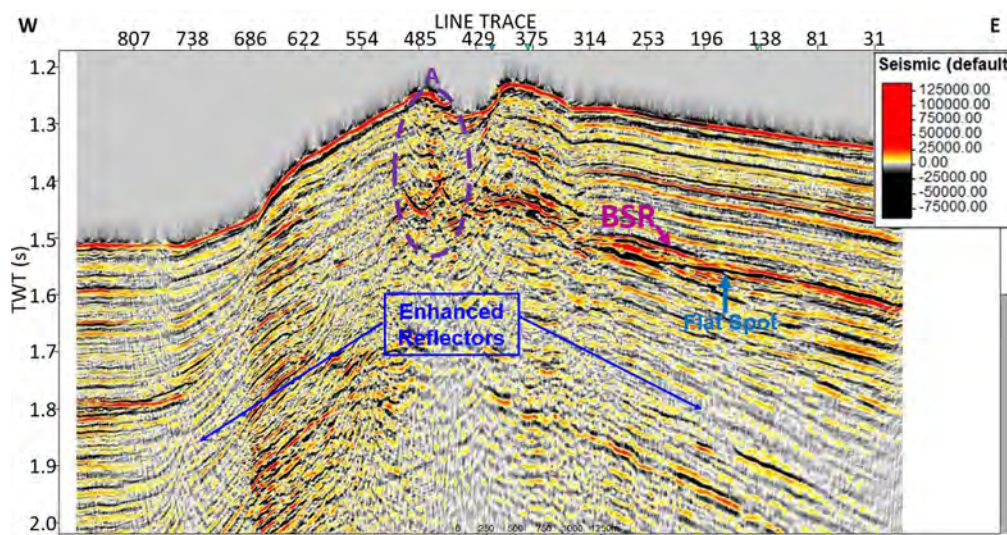


**Figure 7** – SP.2(19\_FSP) with Relative Acoustic Impedance. Arrows point to enhanced reflectors of the blanking zones near the gas chimney. Circle A highlights the non-collapsed diffractions.

### Spectral Decomposition

First, is good to make an analysis of the most dominant frequencies in the area of interest to choose the central frequency of Spectral Decomposition (SD). In this case, the most dominant frequencies were between 100 Hz and 80 Hz, this high frequency band is because the seismic is penetrating a shallow subsurface depth compared for example with typical petroleum targets at

several km below the seafloor. SD is useful to extract detailed stratigraphic patterns with thickness related to dominant frequencies processed with seismic (Laughlin et al., 2002). Thus, to analyze the effects of different Spectral Decomposition using Continuous Wavelet Transform, six distinct central frequencies were applied based on the dominant frequencies of the zone of interest. These frequencies were 25, 50, 75, 100, 125 and 150 Hz (Fig. 8 and Fig. 9).

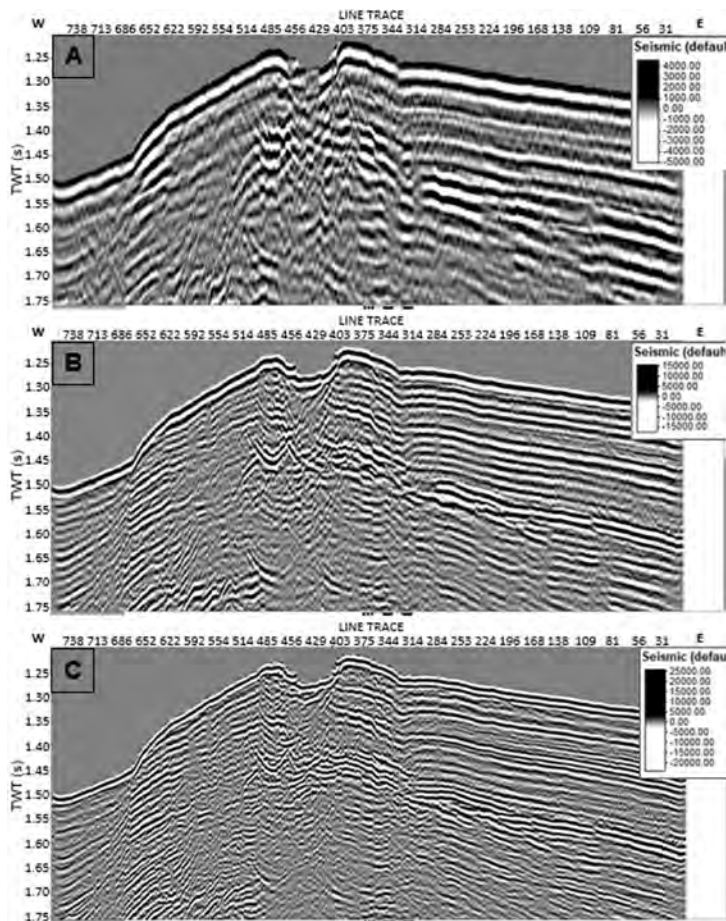


**Figure 8** – Spectral Decomposition of SP.2(19\_FSP) with (A) 25 Hz; (B) 50 Hz and (C) 75 Hz.



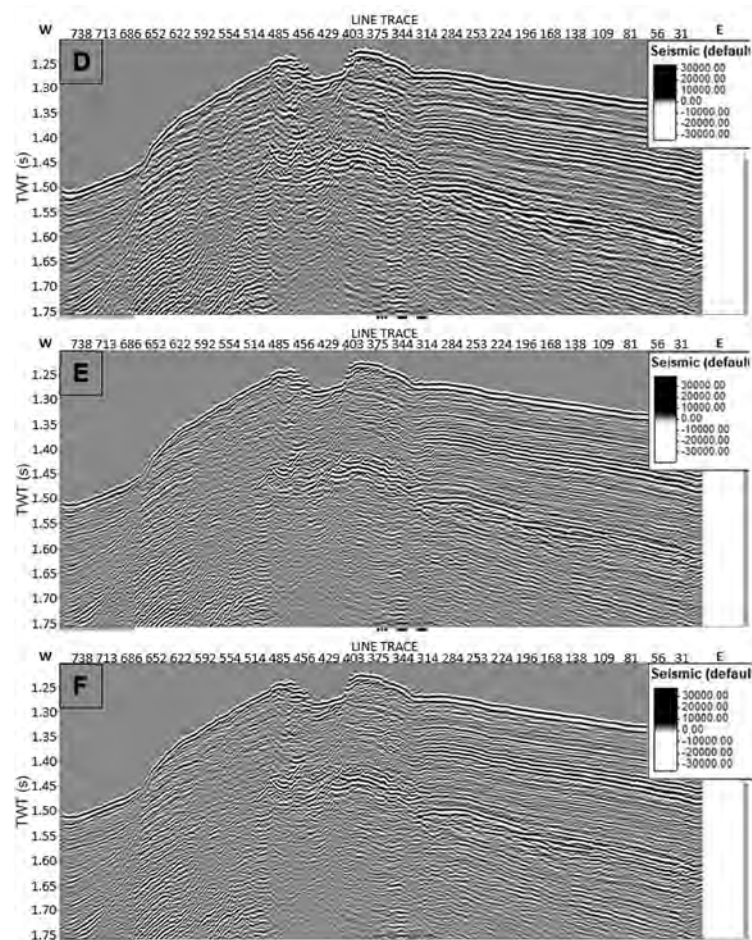


**Figure 9** – Spectral Decomposition of SP.2(19\_FSP) with (D) 100 Hz; (E) 125 Hz and (F) 150 Hz.

All images are on the same scale (Fig. 8 and Fig. 9, A to F). Apparently, it seems that the image corresponding to the SD with a frequency of 25 Hz is with a big zoom, because the seismic reflectors seem to be thicker. This is due to the tuning effect of thin bed interference. In thin reservoirs a lower dominant frequency would highlight the thicker parts on an amplitude map (Laughlin et al., 2002), in this case, seismic sections, and this is what happened when choosing a central frequency of 25 Hz. While seismic data with a higher dominant frequency highlight the thinner parts of the reservoir on seismic sections, as seen in Figure 9 E-F. Thereby, from A to F, we have the illusion that the scale is increasing, but in fact it is the same, what changed was the frequency parameters of the Spectral Decomposition.

After that, to highlight the energies, the Envelope attribute was applied on these results (Fig.10 and Fig. 11). Note that SD with a frequency of 25 Hz has red spots below the pockmark and below the BSR. These spots are probably related to the high impedance contrast generated by the presence of free gas. Thus, for a more detailed investigation of seismic attenuation, instantaneous frequency must be applied.

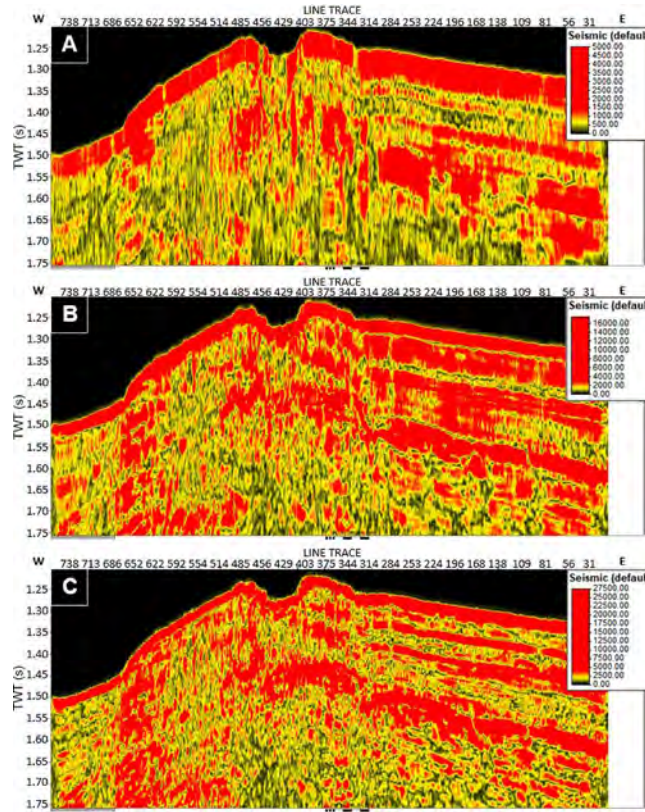


**Figure 10** – Spectral Decomposition plus Envelope of SP.2(19\_FSP) with (A) 25 Hz; (B) 50 Hz and (C) 75 Hz.

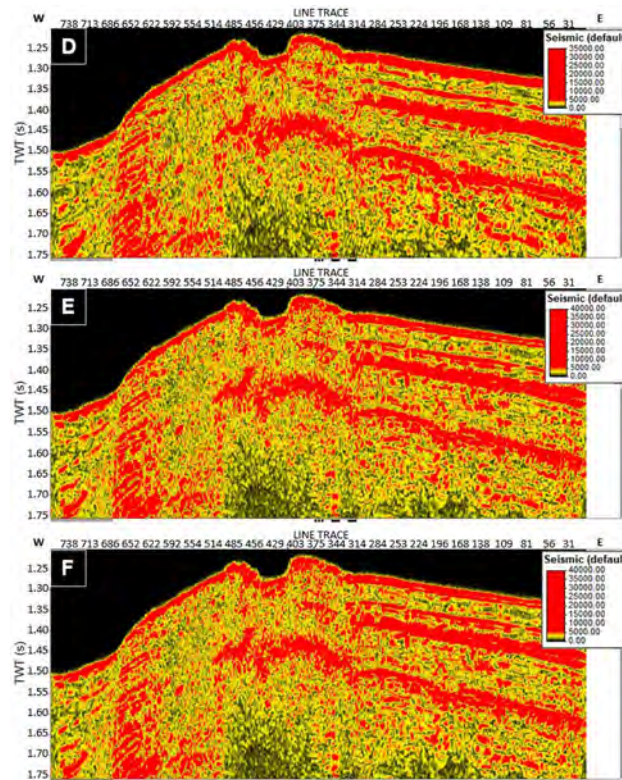


**Figure 11** – Spectral Decomposition plus Envelope of SP.2(19\_FSP) with (D) 100 Hz; (E) 125 Hz and (F) 150 Hz.

### Instantaneous Frequency

After applying Instantaneous Frequency, it is possible to notice that there is a greater dominance of the lower frequencies in the deeper areas (Fig. 12). These red spots may occur due to the high flow of methane from deep sources. This interpretation can be made based on previous studies of geochemical analysis, where these gas chimneys are occasionally associated with seafloor methane seeps and gas plume (Matsumoto et al., 2005; Matsumoto et al., 2009). For instance, based on Freire et al. (2011) interpretation, we can relate the seismic attenuation in the seismic section SP.2(19\_FSP) with the presence of gas, which migrates vertically through faults and laterally through carrier beds (Fig. 12). Besides that, note that the red spots between 2.0 s and 2.4 s correspond to the previous observed blanking zones seen in Figure 2. The high flow of methane from deep sources should attenuate the seismic signal causing this effect.

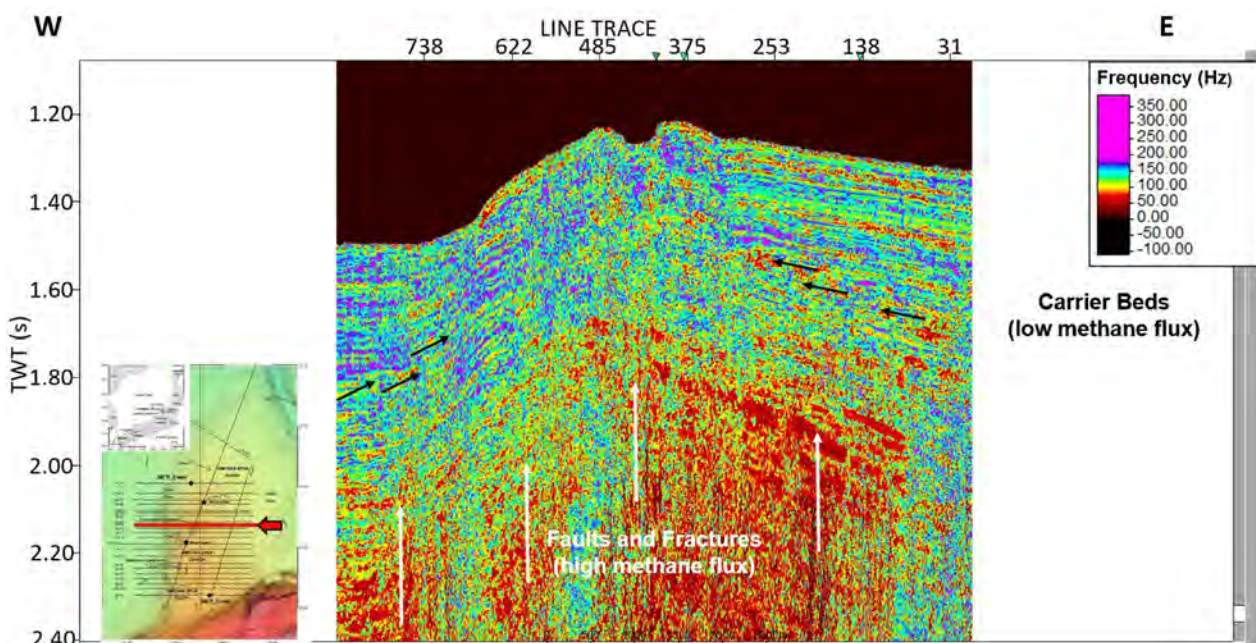


**Figure 12** – SP.2(19\_FSP) with Instantaneous Frequency seismic attribute. Red, yellow and green spots represent frequency values close to 0 Hz, 50 Hz and 100 Hz, respectively. While purple spots represent frequency values approximately greater than 175 Hz (higher frequency values). Black arrows correspond to the low methane flux through carrier beds while white arrows show the high methane flux from deep sources through faults.

In addition, blue and purple spots represent regions with less seismic attenuation. So, since the gas hydrates only exist within the Gas Hydrate Stability Zone (GHSZ), only the purple and blue spots above the BSR could mean their presence in the sediments. So, the purple and blue zones below BSR should represent more compacted sediments because the seismic attenuation is smaller. Thereby, considering these observations and zooming in on the shallow central part, the

interpretation of Figure 13 can be made. Note that the purple spot above BSR could mean gas hydrates sealing the free gas zone just below it (red spot highlighted by white rectangle).

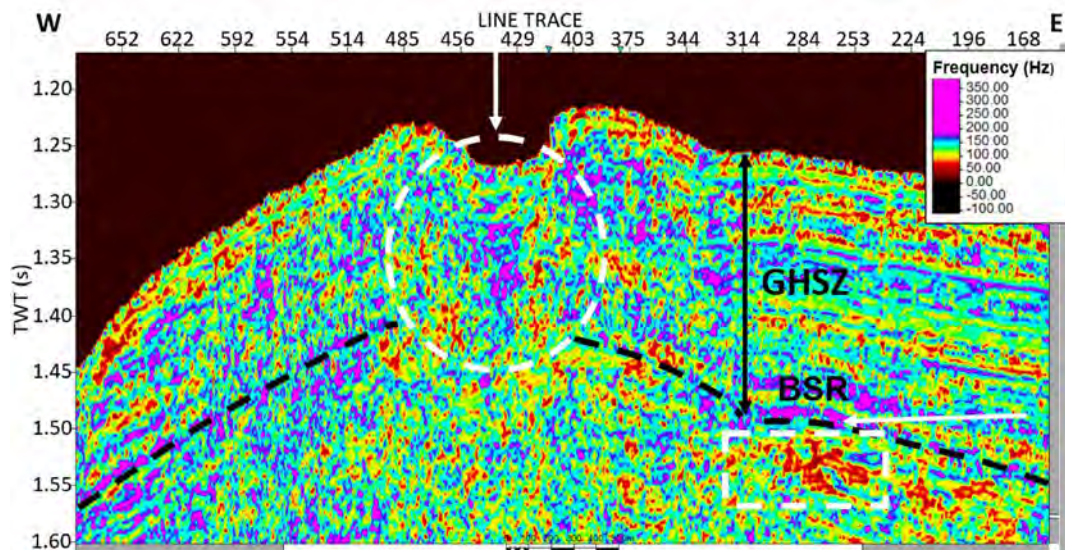


**Figure 13** – SP.2(19\_FSP) with Instantaneous Frequency seismic attribute. Black, red, yellow and green spots represent frequency values close 0 Hz, 50 Hz, 100 Hz and 125 Hz, respectively. While purple spots represent frequency values approximately greater than 175 Hz. White rectangle highlights a higher seismic attenuation below BSR, while white circle highlights possible presence of gas hydrates (purple spots) with free gas (red spots) below the pockmark or these red spots could be related to the faults that could be causing this decrease in frequency, where it has the non-collapsed diffractions seen in the central part of theseismic section SP.2(19\_FSP).

Moreover, note that there is a large seismic attenuation above BSR in the central part (Fig. 13). This result matches unusual low acoustic velocities observed above BSR in previous work. For instance, Saeki et al. (2009) through a velocity analysis of 3D seismic survey data reported anomalously low velocities (1200-1300 m/s) above the BSR horizon, possible affected by the presence of free gas bubbles (Matsumoto et al., 2009, 2011). These low velocities were also observed by Log-While-Drilling (LWD) data of the Umitaka Spur (Matsumoto et al., 2017), that are not used in this work. Thus, the red and yellow spots above the BSR and below the seafloor may implies that free gas is stable well within the gas hydrate stability zone (GHSZ), probably caused by dehydration of the host sediments after gas hydrate formation, which is quite common around the world. In the region circled by the white hatched circle there may be a mixture of gas-charged and gas-hydrate-charged sediments. The same can be seen in SP.2(51-1\_FSP) (Fig. 14). According to Freire et al. (2011) the presence of faults and fractures result in a strong conduit for free gas migration that enriches the GHSZ sediments with both free gas and gas hydrates.

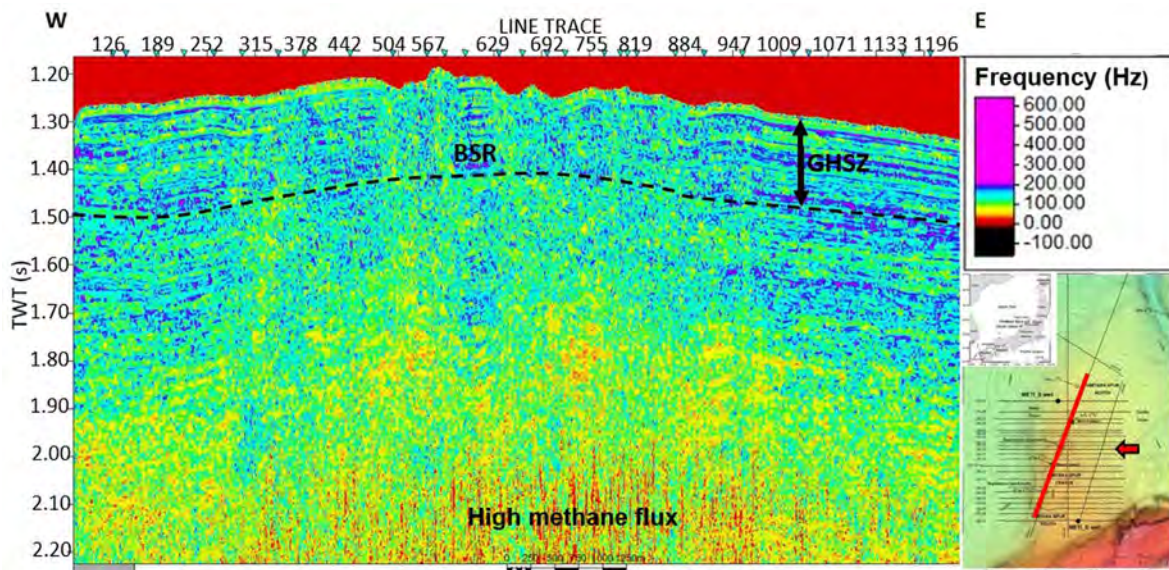


**Figure 14** - SP.2(51-1\_FSP) with Instantaneous Frequency. Red, yellow and green spots represent frequency values close 0 Hz, 50 Hz and 100 Hz, respectively. While purple spots represent frequency values approximately greater than 200 Hz.

### Final interpretation of BSR

After analyzing these six seismic attributes applied, BSR of each seismic profile was interpreted (Fig. 15). It can be seen that the shallow stretches of BSR in red are associated with gas chimneys, where the upward migration of hydrocarbon gases develops gas hydrates accumulations. These zones are also associated with occurrence of mounds and pockmarks (Fig. 1), as noted in previous work (e.g., Matsumoto et al., 2009, 2011, 2017; Freire et al., 2011). Thereby, BSR in gas chimneys ranges from 1.4 to 1.5 s two-way time (about 0.1 TWT below seafloor), while in the surrounding sediments, the depth ranges from 1.6 to 1.8 s TWT (about 0.3 TWT below seafloor).

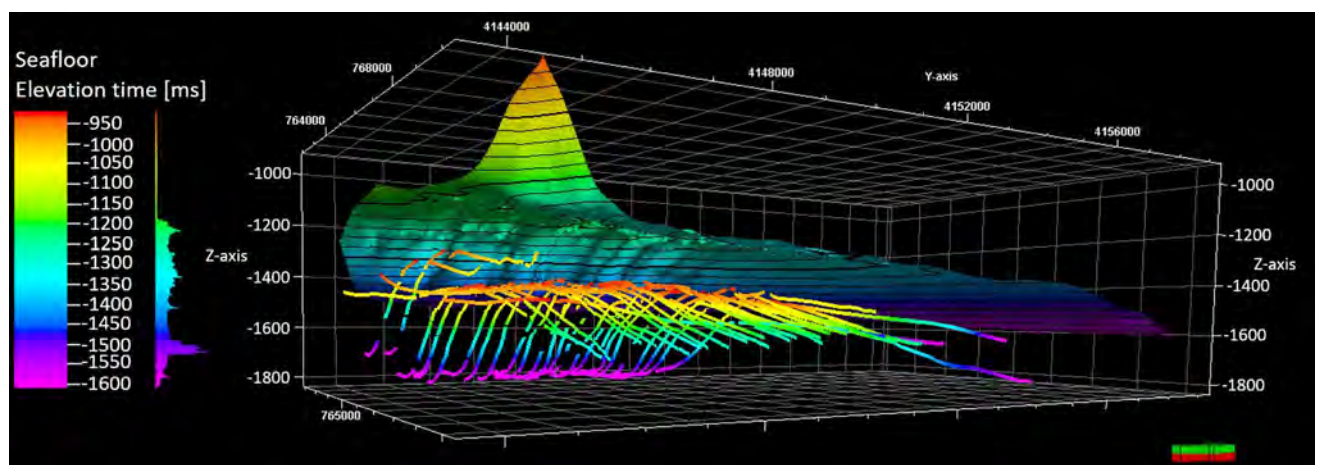


**Figure 15** – Interpreted BSR of each seismic profile below seafloor grid. The color palette refers to elevation in time (ms) of the BSR. Thus, the longer the time, the greater the depth. Red colors correspond to shallow areas (close to 1.4 s TWT) while purple colors represent deeper zones (1.8 s TWT).

### **CONCLUSION**

This study consisted of the application and analysis of seismic attributes to identify Bottom Simulating Reflector (BSR) in the Umitaka Spur gas hydrate province, Joetsu Basin, Japan. Thus, six seismic attributes were applied to twenty-eight single-channel 2D seismic profiles using Petrel software. The Envelope attribute served to highlight the regions of highest amplitude energy. RMS Amplitude generated a result similar to the Envelope, but this attribute was used mainly to apply the Amplitude Volume Technique (tecVA).

Both the tecVA seismic attribute and the Relative Acoustic Impedance served to highlight the impedance contrast of the layers and thus the discontinuities, allowing a better visualization of the geological faults of the seismic sections. The RAI attribute made reflector stronger, thereby reducing the effects of acoustic transparency of free gas zones. While tecVA improves the visualization but hold on all seismic events, the RAI attribute takes off the seismic residual pulse events such as lateral lobes focusing in the geological events. So, both tecVA and RAI work very well together.

Ultimately, the Spectral Decomposition and Instantaneous Frequency were useful to highlight the BSR, which comparatively is like a seismic interface that separates a zone of higher seismic attenuation (free gas zone below) from a milder seismic attenuation (gas hydrates in sediments above). Thus, these seismic attributes were relevant to reduce the ambiguities of the attributes that measure only amplitude.

Therefore, seismic attributes play a fundamental role in the analysis of subsurface layers. Their combination gives security to the interpreter when observing similar results of each one. Thus, the BSR has been interpreted and this work reaffirmed the unusual presence of free gas above the BSR as reported by other studies in this region.

### **ACKNOWLEDGMENTS**

The authors are thankful to Japan Agency for Marine-Earth Science and Technology (JAMSTEC) for providing data from NT07-20 and NT08-09 Expeditions. They are also grateful to Schlumberger, for providing the Petrel Software.

### **REFERENCES**

Aguiar, L. F., A. F. M. Freire, C. G. Silva, and W., Lupinacci, 2021. Identification and analysis of bottom simulating reflectors in the Foz do Amazonas Basin, Northern Brazil. *Brazilian Journal of Geology*, 51(1): e20200075.

- Aguiar L. F., A. F. M. Freire, L. A. Santos, A. C. F. Dominguez, E. H. P. Neves, C. G. Silva, and M. A. C. Santos, 2019, Analysis of seismic attributes to recognize bottom simulating reflectors in the Foz do Amazonas Basin, Northern Brazil. *Brazilian Journal of Geophysics* 37(1):43-53. DOI: 10.22564/rbgf.v37i1.1988
- Aoyama, C., and R. Matsumoto, 2009, Acoustic surveys of methane plumes by Quantitative Echo Sounder in Japan Sea and estimate of the seeping amount of the methane hydrate bubbles. In: Matsumoto R. (Ed), Special Issue on "Methane Hydrate (Part1): Occurrence, Origin, and Environmental Impact". *Journal of Geography* vol 118(1), 156-174. (In Japanese with abstract in English).
- Buffett, B. A., 2000, Clathrate hydrates. *Annual Review of Earth and Planetary Sciences*, 28(1), 477-507.
- Bulhões, É. M., and W. N. Amorim, 2005, Princípio da SismoCamada Elementar e sua aplicação à Técnica Volume de Amplitudes (tecVA). In 9th International Congress of the Brazilian Geophysical Society (pp. cp-160).
- Chong, Z. R., S. H. B. Yang, P. Babu, P. Linga, and X. S. Li, 2016, Review of natural gas hydrates as an energy resource: Prospects and challenges. *Applied energy*, 162, 1633-1652.
- Freire, A. F. M., 2010, An integrated study on the gas hydrate area of Joetsu Basin, eastern margin of Japan Sea, using geophysical, geological and geochemical data. *The University of Tokyo, Graduate School of Frontier Sciences*.
- Freire, A. F. M., R. Matsumoto, and L. A. Santos, 2011, Structural-stratigraphic control on the Umitaka Spur gas hydrates of Joetsu Basin in the eastern margin of Japan Sea. *Marine and Petroleum Geology*, 28(10), 1967-1978.
- Hato, M., T. Matsuoka, T. Inamori, and T. Saeki, 2006, Detection of methane-hydrate-bearing zones using seismic attributes analysis. *The Leading Edge*, 25(5), 607-609.
- Hirai, A., S. Okada, S. Wakamatsuya, Y. Miyamoto, and K. Hachinohe, 1995, Organic geochemical relationship between pooled oils and distribution of their source rocks in the Niigata basin, Japan. *Sekiyu Gijutsu Kyokaiishi*, v. 60, n. 1, p. 87-97.
- Joshi, A.K., L. Pandey, and K. Sain, 2017, Identification of BSR and estimation of gas hydrate from well-log data at NGHP-01-04 and 11A in the Krishna-Godavari Basin, Eastern Indian Margin. 2017 SEG International Exposition and Annual Meeting. Society of Exploration Geophysicists. Expanded abstracts 3483-3487.
- Kvenvolden, K. A., 1993. Gas hydrates—geological perspective and global change. *Reviews of*

geophysics, 31(2), 173-187.

Laughlin, K., P. Garossino, and G. Partyka, 2002, Spectral decomposition applied to 3D.

Matsumoto, R., 2005, Methane plumes over a marine gas hydrate system in the eastern margin of Japan Sea: A possible mechanism for the transportation of subsurface methane to shallow waters. In Proceedings of the 5th International Conference on Gas Hydrates, Vol. 3, pp. 749-754.

Matsumoto, R., Y. Okuda, A. Hiruta, H. Tomaru, E. Takeuchi, R. Sanno, M. Suzuki, K. Tsuchinaga, Y. Ishida, O. Ishizaki, R. Takeuchi, J. Komatsubara, A. F. Freire, H. Machiyama, C. Aoyama, M. Joshima, M. Hiromatsu, G. Snyder, H. Numanami, M. Satoh, Y. Matoba, H. Nakagawa, Y. Kakuwa, S. Ogihara, K. Yanagawa, M. Sunamura, T. Goto, H. Lu, and T. Kobayashi, 2009, Formation and collapse of gas hydrate deposits in high methane flux area of the Joetsu Basin, eastern margin of Japan Sea. *Journal of Geography-Chigaku Zasshi*, v. 118, n. 1, p. 43-71.

Matsumoto R., B. Ryu, S. Lee, S. Lin, S. Wu, S. Sain, I. Pecher, and M. Riedel, 2011, Occurrence and exploration of gas hydrate in the marginal seas and continental margin of the Asia and Oceania region. *Marine and Petroleum Geology*, v. 28, n. 10, p. 1751-1767.

Matsumoto, R., Y. Kakuwa, G. Snyder, M. Tanahashi, A. Hiruta, T. Oi, S. Ohkawa, H. Tomaru, H. Numanami, C. Shen, and S. Morita, 2017, Occurrence and Origin of Thick Deposits of Massive Gas Hydrates, Eastern Margin of the Sea of Japan Sea. In Proceedings of the 9th International Conference on Gas Hydrates.

Nakajima, T., Y. Kakuwa, Y. Yasudomi, T. Itaki, I. Motoyama, T. Tomiyama, H. Machiyama, O. Okitsu, S. Morita, M. Tanahashi, and R. Matsumoto, 2014, Formation of pockmarks and submarine canyons associated with dissociation of gas hydrates on the Joetsu Knoll, eastern margin of the Sea of Japan. *Journal of Asian Earth Sciences*, v. 90, p. 228-242.

Okui, A., M. Kaneko, S. Nakanishi, N. Monzawa, and H. Yamamoto, 2008, An integrated approach to understanding the petroleum system of a frontier deep-water area, offshore Japan. *Petroleum Geoscience*, v. 14, n. 3, p. 223-233.

Oliveira, O. M. V., and S. A. M. Oliveira, 2009, Aplicação Da decomposição espectral de dados sísmicos no estudo das acumulações de hidratos de gás da bacia de Pelotas. In 11th International Congress of the Brazilian Geophysical Society & EXPOGEF 2009, Salvador, Bahia, Brazil, 24-28 August 2009 (pp. 870-874). Society of Exploration Geophysicists and Brazilian Geophysical Society. DOI: 10.3997

Otofuji, Y., T. Matsuda, and S. Nohda, 1985, Paleomagnetic evidence for the Miocene counter-clockwise rotation of Northeast Japan—rifting process of the Japan Arc. *Earth and Planetary Science*



Letters, v. 75, n. 2-3, p. 265-277.

Saeki, T., M. Hayashi, T. Furukawa, T. Inamori, and E. Asakawa, 2009, 3D seismic velocity structure below mounds and pockmarks in the deep water southwest of the Sado Island. In: AGU Fall Meeting Abstracts. p. OS43C-02

Santos, L. A., A. F. M. Freire, R. Matsumoto, 2009, Q estimation in hydrate bearing sediments at Joetsu Knoll Japan Sea. In: 11th International Congress of the Brazilian Geophysical Society. European Association of Geoscientists & Engineers. p. cp-195-00261.

Sato, O., M. Funayama, and H. Annaka, 1987, Sedimentary facies and porosity properties for sandstone reservoirs in the Kakizaki Oki Structure, Niigata Prefecture, Japan. Journal of the Japanese Association for Petroleum Technology, v. 52, n. 1, p. 58-69.

Son, B., T. Yoshimura, and H. Fukasawa, 2001, Diagenesis of dioctahedral and trioctahedral smectites from alternating beds in Miocene to Pleistocene rocks of the Niigata Basin, Japan. Clays and Clay Minerals, v. 49, n. 4, p. 333-346.

Snyder, G. T., R. Matsumoto, Y. Suzuki, M. Kouduka, Y. Kakizaki, N. Zhang, H. Tomaru, Y. Sano, N. Takahata, K. Tanaka, S. A. Bowden, and T. Imajo, 2020, Evidence in the Japan Sea of microdolomite mineralization within gas hydrate microbiomes. Scientific reports, v. 10, n. 1, p. 1-13.

Suzuki, U., 1979, Petroleum geology of the Sea of Japan, Northern Honshu. Journal of the Japanese Association of Petroleum Technologists, v. 44, p. 291-307.

Takeuchi, A. Recent crustal movements and strains along the eastern margin of Japan Sea floor. Geology and Geophysics of the Japan Sea, v. 1, p. 385-398, 1996.

Taner, M. T. 2001. Seismic attributes: Canadian Society of Exploration Geophysicists Recorder. CSEG Recorder, September Issue, p. 48-56.

Taner, M. T., F. Koehler, and R. E. Sheriff, 1979, Complex seismic trace analysis. Geophysics, v. 44, n. 6, p. 1041-1063.

**Neves E.H.P.:** main researcher; **Silva Silva C.G.:** specialist in seismic interpretation; **Matsumoto R.:** Gas hydrate specialist; **Freire A.F.M.:** main advisor, reviewer, gas hydrate specialist.